A contribution to the problem of mapping seabed transition zones.

Laure Amate
Lab. I3S, Sophia Antipolis, France
Email: amate@i3s.unice.fr

Maria-João Rendas
Lab. I3S, Sophia Antipolis, France
Email: rendas@i3s.unice.fr

***Abstract*— The paper proposes a framework for discriminating between distinct sea-bottom regions on the basis of the *shape* of the objects present on them. Supervised (Bayesian) and unsupervised algorithms are presented that allow the definition of *shape classifiers*. These classifiers define partitions of a non-Euclidean shape space which is an extension that imposes robustness with respect to circular permutations and mirroring, additionally to the translational, scale and rotational invariances already contemplated by the original Kendall definition. The algorithms proposed are applied to real data corresponding to the shapes induced on side-scan images by two kinds of underwater bottoms: sand ripples and posidonia fields. Application of the proposed theory to the problem of on-line bottom discrimination is illustrated on fields simulated using statistical shape models identified from real data.**

I. Introduction

Navigation and positioning of autonomous underwater vehicles is usually based on auxiliary systems such as GPS and acoustic buoys. These solutions require either frequent returns to surface for GPS fixes or expensive and time-consuming preparation of the mission site. Alternatively, exclusive use of inertial sensors leads to a constant growth of the positioning error that can result in robot's loss. A solution to this problem is to use a map of the workspace to which the robot refers to estimate its position. This is known as the SLAM problem (Simultaneous Localization And Mapping), and its formal solution is known to be an optimal non-linear smoother, that recursively propagates the joint distribution of the platform trajectory and of the detected environment elements [4].

To be useful for positioning purposes, the map elements must be stable (i.e., re-observable with high probability) and non-ambiguous. This is generally not the case for point-like features, such as isolated strong Sonar returns. Alternatively, some authors considered map environments that describe the workspace using simple parametric forms (lines, planes,...). The environment is then still described by a set of real values, while overcoming the stability/ambiguity problems associated to point features. Unfortunately, the objects that can be found in the ocean environment have a high complexity, and their geometry can seldom be described by simple parametric models. To alleviate these problems, we propose to base robot navigation on the extended geometric natural features of the environment.

We claim that natural benthic contours, that separate distinct regions of the sea floor, are the good candidates as elements of underwater maps. Natural contours correspond rarely to neat boundary lines. More generally, they correspond to transition regions of nonzero width between sea floor regions with distinct statistical characteristics. The problem of acquiring maps of these loosely defined contours has been addressed in [6], resorting to optimal tests for detecting abrupt changes in spatial stochastic parametric models that are fitted to the observed regions. The statistical models used consider randomly scattered objects of random shape (Random Closed Set models). Actually, in this first application of this formalism, random shapes were obtained by randomizing the parameters of simple geometric forms (e.g., circles of random radius). The work presented in this paper, addressing the problem of discriminating between the shapes observed in distinct regions of the sea floor, is a contribution to the definition of *more realistic statistical models for the shape of natural objects*.

Motivated by the idea that the information about contours's shape should be invariant with respect to their observation viewpoint, and by the willingness to be able to directly assess the shapes coded in the map, we separate the information relative to size, position and orientation of the observed contours from the description of their *intrinsic shape*. The posterior map distribution is thus factored into the propagation of separate distributions for the contours' shape, and for their metric/geographic attributes (position, scale and orientation). The resulting notion of shape coincides with that introduced by Kendall in [1]. Kendall's shape theory provides thus a formal characterization of the space where we must propagate the posterior distributions.

The paper is organized in the following way. Section II, summarizes the main tools and definitions of shape theory used in our work, and presents the definition of a *circularly invariant shape space*, that, additionally to the invariances already imposed by Kendall, impose circular permutation and 'mirror' invariances. The need for this more complex shape space arises because the origin of the contour as well as the sense of its sampling are arbitrary, and are not intrinsic characteristics of the perceived objects. We extend to the new 'circular shape space' Kendall's definitions of distance and of mean of a set of shapes (as a Karcher mean). We then formulate in Section III the problem of unsupervised partitioning of a given set of shapes, and present an algorithm that is the transposition to our shape space of the common 'k-means' algorithm [5]. The algorithm presented (or its generalization to an arbitrary

number of classes) can be used for off-line seabed habitat mapping. An incremental version of its present version is proposed to solve, directly in the space of the detected object's, the transition detection problem studied in [6]. Section IV evaluates the performance of the unsupervised algorithm and compares its performance to a Bayesian classifier that uses statistical distributions (in the circular shape space) learned from manually labeled data sets. The shapes models identified can also be used to define simulators of underwater scenarios based on previous missions data, for the development and test of observation and navigation strategies in realistic conditions. Section V illustrates this use of the proposed formalism.

II. Definition of a shape

The (discrete) theory of shape, introduced in 1984 by D.G. Kendall [1], defines the shape of an object as **"what is left after removing location, scale and orientation informations from the object"**.

A. Kendall's definition

In Kendall's theory, an object is an *ordered* finite set of points in an *m*-dimensional vector space. The **configuration** X of an object, see eq. (1), is the $k \times m$ matrix of the coordinates of the *k m*-dimensional points (each line is a point). The set of all configurations of *k* points in *m* dimensions is called *the configuration space* and is a $(m \times k)$-dimensional space. Translation information is deleted by removing from X its mass center X_c, see eq. (2). Then, scaling is removed by normalizing the centered configuration, yielding the **preshape** Z given by eq. (3)[1]. The preshape space, $\mathcal{S}_m^k$, is the hypersphere of unit radius in $\mathbb{R}^{m\times(k-1)}$, also denoted by $\mathbb{S}^{m(k-1)}$.

$$X = [x_1\, x_2 \dots x_k]^T, \qquad x_i \in \mathbb{R}^m \tag{1}$$

$$X_c = \frac{1}{k}\sum_{i=1}^{k} x_i, \qquad X_c \in \mathbb{R}^m. \tag{2}$$

$$Z = \frac{X - \mathbf{1}X_c^T}{\|X - \mathbf{1}X_c^T\|}. \tag{3}$$

Finally, orientation information is removed by considering the quotient by the special orthogonal group ***SO(m)***, the set of all rotations in the m-dimensional space. This defines the **shape** of an object, denoted by $[Z]$, as the equivalence class associated with the action (on the right) of ***SO(m)***, see eq. (4). A shape can be represented by any of the preshapes Z in its equivalence class, called **icons**.

$$[Z] = \{Z\ R\ : R \in \textbf{\textit{SO(m)}}\}, \qquad Z \in \mathcal{S}_m^k. \tag{4}$$

The space of all shapes of objects of k points in m dimensions is noted Σ_m^k. Its dimension is $\left(m(k-1) - 1 - \frac{m(m-1)}{2}\right)$.

[1]The notations $\mathbf{1}$ ($\mathbf{0}$) denote constant vectors with all components equal to 1 (0). The dimension of the vector is implicitly defined by the equation in which it appears.

B. Circularly invariant shape

Kendall's definition of shape considers *ordered* set of landmarks. In our case, the automatic detection of a contour produces a list of samples along the continuous contour, with arbitrary sense and origin. Our notion of shape is thus slightly different from Kendall's and we must add to it invariance with respect to circular permutations and 'mirroring' operations, leading to

***Definition** 1: Let X_1, $X_2 \in \mathcal{X}$ be 2 configuration matrices. X_1 and X_2 have the same* circular shape *if and only if:*

$$X_1 = PX_2A + \mathbf{1}\delta^{\mathbf{T}} \tag{5}$$

with A a rotation and scaling operator, δ a (translation) vector, and $P \in \mathcal{P}$, where $\mathcal{P}$ is the group of all circular and 'mirror' permutations defined below.

***Definition** 2: $\mathcal{P}$ is the (finite) subgroup of the group $\mathcal{G}$ of all permutation operators acting on the left in $\mathbb{R}^k$, $\mathcal{P} \subset \mathcal{G}$, generated by*

$$\Delta_1 = \left[\begin{array}{c|c} \mathbf{0} & I_{k-1} \\ \hline 1 & \mathbf{0}^T \end{array}\right], \quad \textit{and } \Delta_2 = \begin{bmatrix} 0 & \cdots & \cdots & 0 & 1 \\ \vdots & \ddots & \ddots & \ddots & 0 \\ \vdots & \ddots & \ddots & \ddots & \vdots \\ 0 & \ddots & \ddots & \ddots & \vdots \\ 1 & 0 & \cdots & \cdots & 0 \end{bmatrix},$$

i.e., each $P \in \mathcal{P}$ can be written as $P = (\Delta_1)^p(\Delta_2)^l$, with $p \in \{1, \dots, k\}$ and $l \in \{0, 1\}$.

Using this definition, we introduce now the **circular shape space** Σ_m^{*k}, as the quotient of Σ_m^k by $\mathcal{P}$. Elements of Σ_m^{*k} are called **circular shapes**.

***Definition** 3:*

$$\Sigma_m^{*k} = \Sigma_m^k/\mathcal{P}. \tag{6}$$

$$[Z]_c \in \Sigma_m^{*k} \Leftrightarrow$$

$$[Z]_c = \{P\ Z\ R\ : P \in \mathcal{P},\ R \in \textbf{\textit{SO(m)}}\}. \tag{7}$$

C. Distance between shapes

We consider now the problem of directly comparing the shapes $[Z_1]_c$ and $[Z_2]_c$ of two objects X_1 and X_2 in the configuration space. To do this we need to define a distance in the non-Euclidean circular shape space Σ_m^{*k} so that it becomes a metric space.
Kendall proposed several definitions of distance in Σ_m^k. We focus here on the 'Procrustes distance' ρ:

$$\rho([Z_1], [Z_2]) = \inf_{R \in \mathbf{SO(m)}} \arg(Z_2\,,\, Z_1\, R), \tag{8}$$

with $[Z_1], [Z_2] \in \Sigma_m^k$, and Z_1 and Z_2 arbitrary icons in orbits $[Z_1]$ and $[Z_2]$. Introduction of invariance with respect to $\mathcal{P}$ requires the extension of ρ to Σ_m^{*k}, as in the following definition.

***Definition** 4: Given 2 preshapes, Z_1 and Z_2, then*

$$D_P([Z_1]_c, [Z_2]_c) = \min_{P \in \mathcal{P}} \rho([Z_1], [P\, Z_2]) \tag{9}$$

with $\rho([Z_1],[Z_2])$ defined in (8) and $P \in \mathcal{P}$, is a well defined distance in Σ_m^{*k}. $\forall \{[Z_i]\}_{i=1}^3 \in \Sigma_m^{*k}$,

$$\begin{aligned} D_P([Z_1]_c,[Z_2]_c) &= 0 \Leftrightarrow [Z_1]_c = [Z_2]_c. \\ D_P([Z_1]_c,[Z_2]_c) &= D_P([Z_2]_c,[Z_1]_c). \\ D_P([Z_1]_c,[Z_3]_c) &\leqslant D_P([Z_1]_c,[Z_2]_c) + D_P([Z_2]_c,[Z_3]_c). \end{aligned}$$

D. Mean shape of a set of shapes

The mean of a finite subset of Σ_m^{*k} can be properly defined as its *Karcher mean*, which is a generic extension of the notion of mean value appropriate for non-Euclidean metric spaces:

***Definition** 5: Let $\mathcal{A} = \{X_i\}_{i=1}^n, \subset \mathcal{X}$, and $d(\cdot,\cdot)$ be a distance in $\mathcal{X}$. The **Karcher mean** of $\mathcal{A}$ is the element $\mu \in \mathcal{X}$ that minimizes the sum of squared distances:*

$$\mu = \arg\min_{X \in \mathcal{X}} \sum_{i=1}^{n} d^2(X, X_i).$$

Using the metric circular shape space $\left(\Sigma_m^{*k}, D_P\right)$, we can define the average circular shape of a collection of objects $\{X_i\}_{i=1}^n$ as the Karcher mean of the corresponding circular shapes $\{[Z_i]_c\}_{i=1}^n$,

$$[\mu]_c = \arg \inf_{[m]_c \in \Sigma_m^{*k}} \sum_{i=1}^{n} D_P^2([Z_i]_c, [m]_c) \tag{10}$$

Notice that $[\mu]_c \in \Sigma_m^{*k}$: the mean of a set of circular shapes is itself a circular shape.

E. Tangent space to a shapes

For practical shape analysis, working in the tangent spaces can be useful. Tangent spaces are linearized versions of the circular shape space in the vicinity of a particular circular shape. They are Euclidean subspaces of the Euclidean space on which the shape spaces are embedded. The tangent space to the preshape sphere at point γ is noted T_γ.
To each $[Z]_c \in \Sigma_m^{*k}$ in a vicinity of $\gamma \in \Sigma_m^{*k}$ we can make correspond a vector $v \in T_\gamma$ as the orthogonal projection of the icon of $[Z]_c$ that is closest (in the sense of the distance D_P) to γ into the linear subspace orthogonal to $\Sigma_m^{\star k}$ at γ.

***Definition** 6: The tangent vector $v \in T_\gamma$ corresponding to $[Z]_c \in \Sigma_m^{*k}$ is:*

$$v([Z]_c) = \left(I_{k-1} - \gamma\gamma^T\right) \widehat{P} Z \widehat{R} \ , \tag{11}$$

where $Z \in [Z]_c$, I_{k-1} is the $(k-1)$ identity matrix, and $\widehat{R} \in \mathbf{SO}(\mathbf{m})$ and $\widehat{P} \in \mathcal{P}$ are the operators that minimize the distances in equations (8) and (9), respectively.

III. Partitioning sets of shapes

Formally, a **classifier** $\mathcal{C}$ is a 1-to-1 mapping from its input space $\mathcal{X}$ to a finite set $\mathcal{H} = \{H_1, \ldots, H_M\}$ of classes:

$$\begin{aligned} \mathcal{C} : \mathcal{X} &\rightarrow \mathcal{H} \\ X &\mapsto \mathcal{C}(X) = H_i, i \in \{1, \ldots, M\} \end{aligned}$$

Define the *decision regions*,

$$R_i = \mathcal{C}^{-1}(H_i) = \{X \in \mathcal{X} \ : \ C(X) = H_i\}, \ i = 1, \ldots, M.$$

Then the collection $\{R_i\}_{i=1}^M$ is a partition of $\mathcal{X}$:

$$\bigcup_{i=1}^{M} R_i = \mathcal{X}, \qquad R_i \cap R_j = \emptyset, \ i \neq j.$$

A classifier is thus formally equivalent to a partition of the input space. In our case, $\mathcal{X}$ is the circular shape space Σ_m^{*k} characterizing the shapes $\{[Z_i]_c, i = 1 \ldots n\}$ of the contours of objects detected on the seabed.

Design of optimal classifiers (that minimize the probability of classification error) requires knowledge of the probability distributions of the observed data under each class. In most practical cases, these distributions are not known, and must themselves be identified from representative labeled data sets $\{\mathcal{L}_i\}_{i=1}^M$ (the *learning sets*, where the true class of each example is known). In some situations (like when detecting a boundary between distinct seabed regions during a mission) these labels are not known in advance, and thus actual classification of the objects (assignment of meaningful labels) is not possible. Alternatively, unsupervised segmentation algorithms can be used to identify – amongst a set of unlabeled objects $\mathcal{L} = \bigcup_{i=1}^M \mathcal{L}_i$ belonging to the M distinct classes – separate groups $\{\mathcal{C}_i\}_{i=1}^M$, each one collecting "similar" objects. Without further knowledge of the features that indeed separate the classes, the measure of resemblance (or distance) used to identify these clusters is normally the uniform (translation invariant) measure in $\mathcal{X}$. Sets $\mathcal{C}_i$ can then be used in the place of the learning sets $\mathcal{L}_i$ to define an (**unsupervised**) classifier. In the next subsection we present the design of a binary unsupervised segmentation algorithm that can be used for off-line map building. A subsequent section presents an incremental version suitable for on-line boundary detection. Since in our case we know the correct label of each member of the learning set used, we compare in a later section the performance of this classifier to the performance of a (**supervised**) Bayes classifier relying on probability distributions directly identified using the sets $\mathcal{L}_i$.

A. Unsupervised classifier

The binary unsupervised classifier presented in this section is a simple *minimum distance* classification algorithm, implementing the decision rule

$$\forall X \in \mathcal{X}, \quad C(X) = H_{j^\star}, j^\star = \arg \min_{j \in \{1,\ldots,M\}} d(X, [M_j]_c). \tag{12}$$

In our case, $\mathcal{X} = \Sigma_m^{*k}$ and $d \equiv D_P$. The parameters $[M_j]_c \in \mathcal{X}$ that implicitly define the decision regions of this classifier are the centroids (in the sense of the Karcher mean in Definition 5) of the clusters $\mathcal{C}_j$ identified by the unsupervised clustering algorithm that is presented below. The decision boundary of this classifier is obviously the low-dimensional variety bisecting the geodesics (in the circular shape space Σ_m^{*k}) that join neighboring $[M_i]_c$ and $[M_j]_c$.

a) Unsupervised clustering: Our algorithm, see Figure 1, is an extension to the non-Euclidean circular shape space of the well known *k-means* algorithm [5]. It alternates between two steps. At iteration r, a class (label) $\ell^r(Z)$ is associated to each data item $Z \in \mathcal{L}$ using the minimum distance criterion (12) for the current centroids $[M_j^{r-1}]_c$. A second step updates the decision boundaries (i.e., the values $[M_j^r]$) by computing the Karcher mean of the new sets $\mathcal{C}_j^r$.

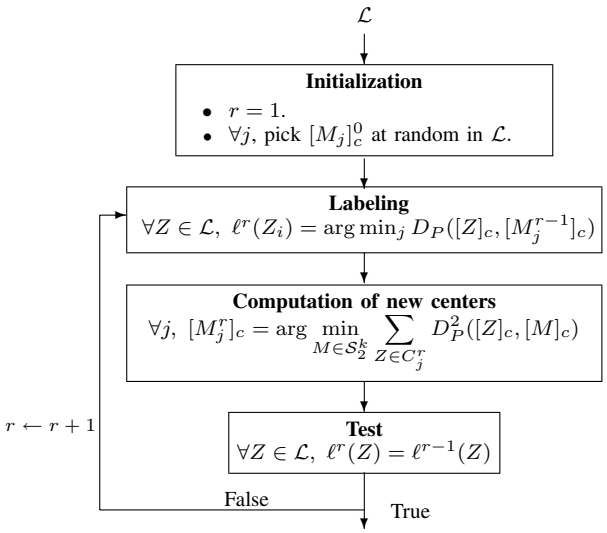

Fig. 1. Block diagram of the unsupervised clustering algorithm.

b) Incremental partitioning: In the context of on-line mapping, we wish to identify the distinct regions of the sea bed as data is progressively acquired,

$$\mathcal{L}_n = \mathcal{L}_{n-1} + \Delta(t_n), \qquad n = 1, 2, \ldots$$

where we denote by $\mathcal{L}_n$ the set of shapes acquired up to time t_n, and $\Delta(t_n)$ represents the set of objects acquired in $]t_{n-1}, t_n]$. We recursively apply the algorithm presented above, see Figure 2, testing, at each cycle, the effective presence of two distinct classes by applying a Hotelling's T^2 test to the classes found [7]. It tests whether 2 sets (with multivariate normal distributions and equal covariance matrices) are separable and if they have equal means.

Let $[M_j]_c^0, j = 1, 2$ be two centroids initialized as for the unsupervised algorithm, and denote by $[M_1]_c, [M_2]_c = \mathcal{C}_u(\mathcal{L}, [M_1]_c^0, [M_2]_c^0)$ the result of applying the three last steps in Figure 1 to the set $\mathcal{L}$ from initial centroids $[M_1]_c^0, [M_2]_c^0$. Denote by $\mathcal{C}_j, j = 1, 2$ the corresponding partition of $\mathcal{L}$. The diagram in shows how the labels of the objects in sets $\mathcal{L}_n$ are iteratively updated.

B. Bayesian classifier

An appropriate measure of the performance of a classifier is the *probability of misclassification*, P_ϵ, which is minimized by Bayesian classifiers. For equiprobable classes, this criterion leads to of the *Maximum Likelihood classifier*:

$$X \leftrightarrow H_{i^\star} \Leftrightarrow p(X|H_{i^\star}) \geq p(X|H_i), \qquad i \neq i^\star\ , \qquad (13)$$

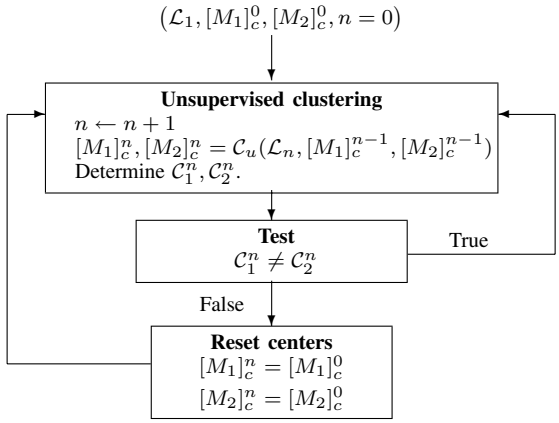

Fig. 2. Incremental partitioning.

where $p(X|H_i)$ is the data distribution for the class i.

To built this classifier we must identify, using labeled learning sets $\mathcal{L}_i$, the probabilistic models $p(X|H_i)$. Usually, this is done considering that $p(X|H_i) \in \mathcal{G}^\theta$, where $\mathcal{G}^\theta$ is some parametric family of distributions indexed by the vector $\theta \in \Theta$. In our case, $X \in \Sigma_m^{*k}$, on which no standard parametric families have been defined. We decide to built *local models* fitting multivariate normal models to projected versions $\mathcal{L}_i^\perp$ of these learning sets, which are obtained by projecting each $\mathcal{L}_i$ orthogonally in the tangent space T_{μ_i} to its Karcher mean $\mu_i \in \Sigma_m^{*k}$. Our models are thus defined by the two first moments of $\mathcal{L}_i^\perp$: their mean and covariance matrix (determined using the usual algebra of multi-dimensional real vector spaces). Figure 3 represents schematically the construction of the Bayesian classifier. We denote the identified distributions by $\hat{p}(v|H_i), v \in \mathcal{L}_i^\perp$.

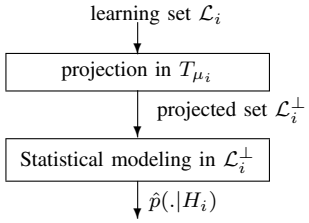

Fig. 3. Learning the statistical models of the learning sets $\mathcal{L}_i$.

Classifier $\mathcal{C}_b$ uses the statistical models $\hat{p}(.|H_i)$ in the *likelihood* test of eq. (13).

IV. Classification of real data sets

The classifiers presented in the previous section are applied to objects detected in Side-Scan SONAR images[2] acquired by an AUV in areas presenting mainly two types of seabed: 'posidonia' fields and regions of sand ripples. Learning sets $\mathcal{L} = \mathcal{L}_{sand} \bigcup \mathcal{L}_{pos}$ have been extracted from those images with shapes of characteristic 'posidonia' clusters ($\mathcal{L}_{pos}$) and shapes of sand ripples ($\mathcal{L}_{sand}$). Figure 4 shows (on the right)

[2]The data used in this section has been provided to us by the NATO Undersea Research Center (La Spezia, Italy)

examples of the contours of 'sand ripple' and contours of 'posidonia'.

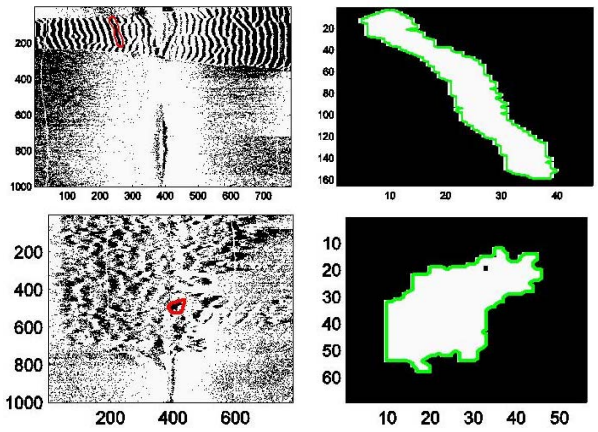

Fig. 4. Side-scan images of 'sand ripples' (top) and 'posidonia' clusters (bottom).

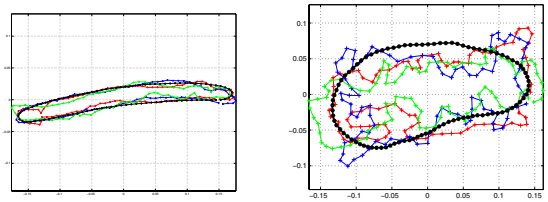

Fig. 5. 3 contours of 'sand ripples' (one color for one object) (on the left) and 3 contours of 'posidonia' clusters (on the right).

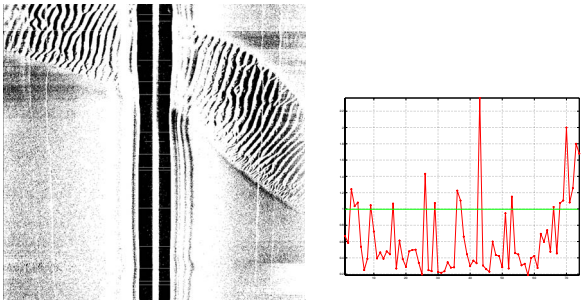

Fig. 6. Side-scan image and ratio of distances between its 74 extracted objects and the mean shapes of "sand ripples" and "posidonia" clusters.

Figure 6 shows a real side-scan image and the result of the classification of its extracted objects: with a ratio of distances below 1 (the green line), 55 out of 74 are classified as "sand ripples", and above the threshold, 19 are classified as "posidonia" clusters.

A. Statistical modeling

To learn the statistical models of each class we use the labeled sets $\mathcal{L}_i, i \in \{pos, sand\}$. We start by computing their (Karcher) mean shapes $[\mu_i]_c, i \in \{pos, sand\}$, which are plotted in Figure 5, superimposed on 3 typical members of the corresponding sets.

Elements of $\mathcal{L}_i, i \in \{pos, sand\}$ are then projected onto T_{μ_i}, yielding the sets $\mathcal{L}_i^{\perp}$. Multivariate Gaussian models are then identified in these Euclidean spaces, by determining the sample mean and covariance matrices $\Sigma_i, i \in \{pos, sand\}$ of the sets $\mathcal{L}_i^{\perp}$. We verify that the (Euclidean) mean of the elements of $\mathcal{L}_i^{\perp}$ is close to zero, as expected. For illustration, the covariance matrix Σ_{sand} is displayed in Figure 7. It can be seen that structure of the covariance matrix agrees well with the symmetry characteristics of this set: the x and y coordinates are weakly correlated (off-diagonal blocks), while there is a periodic correlation of the x coordinates, related to the "bean-like" shape of the sand-ripples.

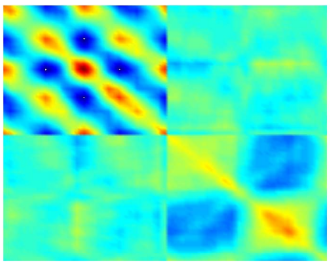

Fig. 7. Covariance matrix Σ_{sand}.

B. Unsupervised clustering

On Figure 8 we represent the centroids $[M_i]_c$ of the classes $\mathcal{C}_i, i = 1, 2$ found by the algorithm $\mathcal{C}_u$ presented in section III-A, superimposed with their elements.

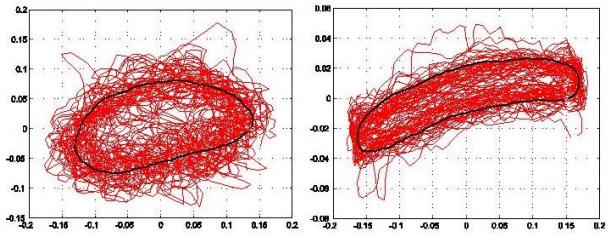

Fig. 8. $\mathcal{C}_1, \mathcal{C}_2$ (in red), and mean shapes $[M_1]_C$, $[M_2]_C$(in blue).

Figure 9 displays for $[Z]_c \in \mathcal{L}$ the ratios $D_P([Z]_c, [M_2]_c)/D_P([Z]_c, [M_1]_c)$. The red line is the unit threshold: objects below it are associated to $\mathcal{C}_2$ and those above to $\mathcal{C}_1$. Objects have been numbered consecutively in $\mathcal{L}_{sand}$ and $\mathcal{L}_{pos}$ such that $X_i \in \mathcal{L}_{sand}, i \leq 152$ and $X_i \in \mathcal{L}_{pos}, 152 < i \leq 312$. These results show that we can reliably associate $\mathcal{C}_1 \equiv \mathcal{L}_{pos}$ and $\mathcal{C}_2 \equiv \mathcal{L}_{sand}$.

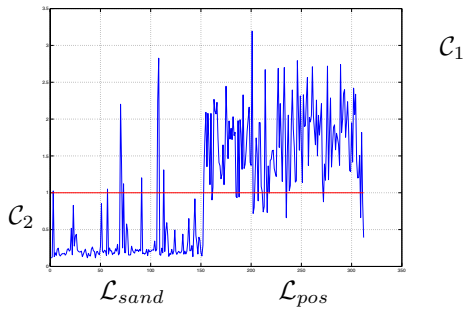

Fig. 9. Ratio of distances between elements of $\mathcal{L}$ and $[M_1]_c$ and $[M_2]_c$.

C. Performance comparison

We compare now – using test sets $\mathcal{T}_i, \neq \mathcal{L}_i, i \in \{pos, sand\}$ with sizes $|\mathcal{T}_{pos}| = 60$ and $|\mathcal{T}_{sand}| = 30$ – the performances of $\mathcal{C}_u$ – presented in section IV-B – and $\mathcal{C}_b$ – defined by the local normal models $\hat{p}(v|H_i)$, see section IV-A). We observed the following classification errors:

$$\Pr\{\text{error}|\mathcal{T}_{pos}\} = 0, \qquad \Pr\{\text{error}|\mathcal{T}_{sand}\} = 0.1\ ,$$

leading to an average percentage of errors equal to 3.3%.

Figure 10 plots, for $[Z]_c \in \mathcal{T}_{sand} \cup \mathcal{T}_{pos}$, the ratio $D_P([Z]_c, [M_2]_c)/D_P([Z]_C, [M_1]_c)$. Note that the centroids $[M_i]_c$ are those identified in section IV-B using the unlabeled set $\mathcal{L}$. As before, the red line is the decision threshold.

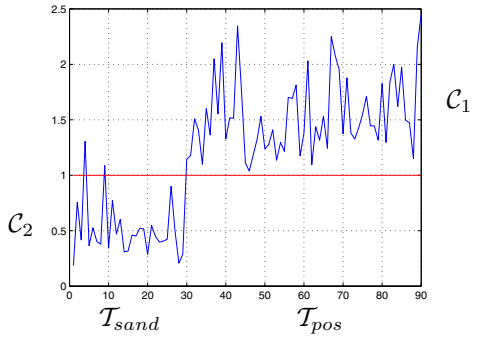

Fig. 10. Results of the $\mathcal{C}_u$ on $\mathcal{T}_{sand} \cup \mathcal{T}_{pos}$.

Figure 11 plots the *log likelihood ratio* of the Bayes classifier $\mathcal{C}_b$ that uses the models identified in section IV-A, over the same test set as in Figure 10. The decision threshold is now equal to zero, as indicated by the red line.

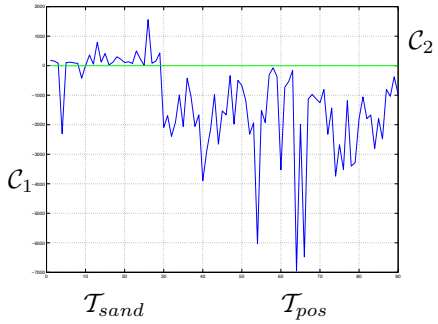

Fig. 11. Results of $\mathcal{C}_b$ on $\mathcal{T}_{sand} \cup \mathcal{T}_{pos}$.

The confusion matrix obtained coincides with that of $\mathcal{C}_u$. This analysis shows thus that, within the limitations of our local statistical modeling approach, the simpler minimum distance classifier identified by unsupervised partition of an unlabeled set of shapes is nearly optimal, indicating the possibility of designing on-line algorithms for the active mapping of boundaries between these two types of seabed regions.

V. Simulation

In this section we use the shape models $\hat{p}(v|H_i), i \in \{pos, sand\}$ identified in section IV-A to simulate pre-processed side-scan images of the seabed. We consider that the region of analysis $\mathcal{A}$ is partitioned in sub-regions $\{\mathcal{A}_k\}_{k=1}^K$. In each $\mathcal{A}_k$, the environment follows a *Random Closed Set* model [6] that characterizes the corresponding type of seabed.

Random Closed Set models are double stochastic models of spatial random fields. Let $\mathcal{A}_k$ be the region of analysis. First, a realization $\{p_i^k\}_{i=1}^{N^k}$ of a point process with intensity function $\lambda^k(p), p \in \mathcal{A}_k$ is generated. A random sample of the spatial field, $\mathcal{M}_k$, is then generated by placing at each point p_i^k, a realization X_i^k of a random *shape process*:

$$\mathcal{M}_k = \bigcup_{i=1}^{N^k} p_i^k \oplus X_i{}^k,$$

where $v \oplus A$ denotes the translation of set A by vector v.

The random objects are generated according to:

$$X_i^k = \alpha_i^k R_{\theta_i^k} Z_i^k,$$

where $\alpha_i^k > 0$ is a random scale factor drawn from $p^k(\alpha)$, $R_\theta \in \mathbf{SO(2)}$ is a rotation matrix, $\theta_i^k \in [0, 2\pi]$ is a random orientation drawn from $p^k(\theta)$, and Z_i^k is a random shape, drawn from one of the models identified in section IV-A. Figure 12 shows a simulated scenario.

Fig. 12. Simulated seabed.

Future publications will consider the use of these models for autonomous mapping of seabed transition zones.

References

[1] D.G. Kendall *Shape manifolds, Procrustean metrics and complex projective space*, Bull. London Math. Soc., 1984, pages 81-121.

[2] J.J. Leonard and H.F. Durrant-Whyte *Simultaneous Map Building and Localization for an Autonomous Mobile Robot*, IEEE/RSJ IROS'91, Osaka, Japan, 1991.

[3] M.J. Rendas and S. Rolfes *Using Non-Linear Filtering Techniques for Robot Localization in Sparse Environments using Perceptual Sensors*, Proceedings of the 7th International Symposium on Intelligent Robotics Systems, Coimbra, Portugal, July 1999.

[4] M.W. M.G. Dissanayake, P.Newman, H.F. Durrant-Whyte, S.Clark, and M.Csorba *A solution to the simultaneous localization and map building (SLAM) problem*, IEEE Transactions on Robotic and Automation, 17(3):229–241, June 2001.

[5] J. MacQueen *Some methods for classification and analysis of multivariate observations*, Proceedings Fifth Berkeley Symposium on Math. Stat. and Prob., pages 281-297, 1967.

[6] S. Rolfes *Stochastic geometry : an approach to featureless perception-based robot navigation*, PhD thesis, December 2002.

[7] I.L. Dryden and K.V. Mardia *Statistical Shape Analysis*, John Wiley & sons, Ltd, 1998.